JOURNAL OF AIRCRAFT
Vol. 47, No. 6, November–December 2010

Flight Control Using Wing-Tip Plasma Actuation

Gilles Boesch,* Huu Duc Vo,† Bruno Savard,‡ Christelle Wanko-Tchatchouang,‡ and Njuki W. Mureithi§
École Polytechnique de Montréal, Montréal, Québec H3T 1J4, Canada

DOI: 10.2514/1.44003

A concept for lift modification on a conventional aircraft wing for roll control at low angle of attack with dielectric barrier discharge plasma actuators is proposed and assessed through computational fluid dynamics simulations and preliminary wind-tunnel experiments. The concept consists of placing plasma actuators around the wing tip to add momentum in the direction opposite to that of the flow forming the tip vortex. Because of the limited strength of existing plasma actuators, the assessment is carried out for a relatively small two-dimensional wing (NACA 4418) with a rounded tip at zero angle of attack and 15 m/s for a Reynolds number in the range of 1.5×10^5. Computational fluid dynamics simulations show a significant alteration of the vorticity field downstream of the trailing edge characterized by a more diffused vortex surrounded by zones of negative vorticity induced by the actuators and, but not necessarily, outboard displacement of the tip vortex. This leads to a reduced downwash that results in a change in lift of up to almost 20% for actuator strength levels that should be achievable in the short term with a new generation of dielectric barrier discharge actuators. The actuator placed on the suction side contributes the most to the lift increase, with its induced jet blocking the flow around the wind tip at the origin of the formation of the tip vortex. Wind-tunnel experimental results support the computational fluid dynamics predictions in both magnitude and trend. Furthermore, preliminary computational fluid dynamics simulations are carried out for a symmetric nonlifting wing (NACA 0018), representative of aircraft tail surfaces at zero angle of attack to generate lift for pitch and yaw control. Results indicate lift generation that increases and becomes larger than drag at higher actuator strengths. These promising results show a potential for the proposed concept to replace movable flight control surfaces on future aircraft wings and empennages.

I. Introduction

CONTINUING pressure in the aviation industry toward reduced acquisition and operating costs drives aircraft design toward reduced weight and complexity. The movable flight control surfaces (namely, the ailerons, elevators and rudder, and their associated systems) constitute a source of weight and mechanical complexity. The replacement of these surfaces with static flight control devices could potentially lead to simpler and lighter wing and tail empennage designs with increased fuel containment capacity, resulting in longer flight range while reducing fabrication and maintenance costs. Recent advances in aerodynamic actuators for flow control provide unprecedented opportunities to develop new practical and robust flight control technology.

Plasma actuators form a new simple and potentially robust electrofluidic actuation technology that allows one to add momentum in near-surface flows. Figure 1 illustrates the workings of a dielectric barrier discharge (DBD) actuator, the most common type of plasma actuator. It basically consists of two axially offset electrodes, one exposed to the air and the other hidden in a dielectric material. When a relatively low-power AC voltage of typically several kilovolts and several kilohertz is applied between the electrodes, the air over the hidden electrode is partially ionized and, in presence of the electric field between the electrodes, results in the acceleration of a thin layer of flow adjacent to the surface. More details on DBD actuators can be found in [1]. Being electric and devoid of moving parts, plasma actuators can be potentially robust and easy to integrate with higher bandwidth than most mechanical actuators. Moreover, the possibility of having the exposed electrode flush with the surface eliminates the risk of negatively perturbing the flow when the actuator is not in use. Consequently, plasma actuators hold a very high promise for flow control applications in aerospace, particularly those involving boundary-layer separation, such as maintaining airfoil lift at high angle of attack [2,3] and preventing flow separation on turbine blades [4] and diffuser walls [5]. Other applications in propulsion include suppressing tip clearance flow in turbines [6] and rotating stall in compressors [7].

The use of plasma actuators for electric flight control without traditional moving surfaces has received recent attention with the work on a swept-wing unmanned aerial vehicle (UAV)-shaped platform [8,9]. The concept consists of altering the lift on wings and stabilizers to provide roll, pitch, and yaw control. At high angle of attack, this concept relies on influencing the leading-edge separation vortices to change the lift and provide rolling moment. At low angle of attack, a ramp is built onto the wing surface to induce separated flow, implying a possible drag penalty under normal flight, and plasma actuators are used to suppress this flow separation to provide the required change in lift for rolling moment.

The objective of this paper is to propose and study computationally and experimentally a method for altering lift using plasma actuators on a conventional wing at low angle of attack in the absence of any imminent boundary-layer separation, with a preliminary assessment of extending the method to generate lift on symmetric tail surfaces. Figure 2 illustrates the proposed concept. It consists of placing plasma actuators near the tip of the wing, both on the suction and pressure sides and if needed on the wing-tip surface to add momentum in the direction opposite to the flow around the wing tip forming the tip vortex. The intent is to impede the development of the tip vortex to alter streamwise vorticity distribution downstream of the trailing edge. This alteration could include displacement of the tip vortex, making it more diffuse and inducing negative vorticity, to reduce downwash upstream of the wing and thus increase lift for roll control (and reduce induced drag). By extension, the same concept could perhaps be applied to potentially create tip vortices on symmetric nonlifting tail surfaces to generate lift in either direction for yaw and pitch control.

Received 23 February 2009; revision received 30 April 2010; accepted for publication 4 May 2010.

*Graduate Student, Department of Mechanical Engineering; currently Engineer, GPCO, Inc., Varennes, Québec, Canada.
†Associate Professor, Department of Mechanical Engineering. Member AIAA (Corresponding Author).
‡Undergraduate Student, Department of Mechanical Engineering.
§Professor, Department of Mechanical Engineering.

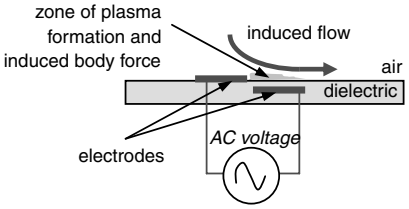

Fig. 1 DBD plasma actuator.

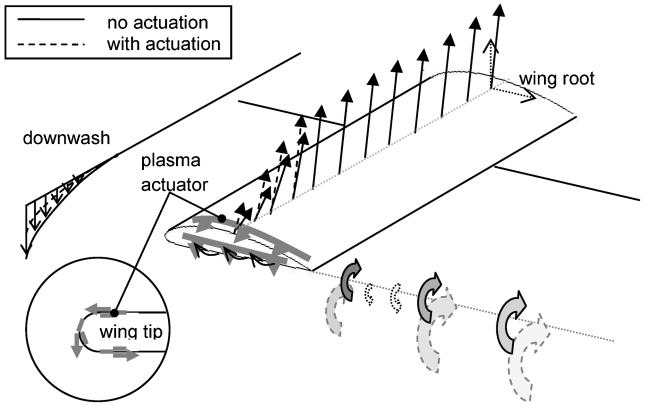

Fig. 2 Proposed concept of lift enhancement via wing-tip plasma actuation.

Studies on control of wing-tip vortices in order to influence lift and drag have been carried out for several decades using jet injection [10–15], suction [16], and synthetic jets [17]. These studies are usually carried out with small wings in wind-tunnel experiments and have reported positive results, with most of them involving spanwise injection for which the increase in lift occurred mainly through the outward spanwise displacement of the tip vortex. Despite their encouraging results, some practical drawbacks of these air systems could impede their applications on aircraft. For air injection systems, these include the jet mass flow (diverted from the engine), which may have an effect on aircraft/engine performance, as well as the mechanical/weight and maintenance issues associated with the required valve/piping systems. For the suction systems, in addition to the drawback associated with valve/piping systems, a source of vacuum would not be easily found on an aircraft. Finally for synthetic jets, there is a maintenance concern associated with the risk of clogging from particles in the dirty air. The use of plasma actuators, by their solid-state and electrical nature, may overcome these drawbacks as well as provide a potentially robust and fast-response method for flight control. Ramakumar and Jacob [18] and Santhanakrishnan et al. [19] briefly tested and discussed spanwise plasma actuation near the wing tip as part of several lift enhancement technologies. Their results were limited to very low Reynolds number (30,000) and extreme angles of attack (14°), which has only limited usefulness in the present context, and especially considering that at high angles of attack where there is higher risk of boundary-layer separation, streamwise plasma actuation on the suction side [2,3] may have more effect on lift.

In contrast, the proposed concept and associated placement of the plasma actuators combines both injection and suction effects to diminish the negative influence of the tip vortex without necessarily being limited to displacing it. Nevertheless, given the very thin region of plasma-induced flow and the relatively low strength of existing plasma actuators, the questions that must be answered in this preliminary assessment are as follows:

1) Can this concept effectively increase lift on a conventional wing at zero angle of attack?

2) Can this concept be extended to generate lift on a symmetric wing?

A computational approach combined with preliminary wind-tunnel experiments is chosen to provide a preliminary assessment and answer to the above questions. As plasma actuators are a relatively new technology and still very much at the laboratory stage of development, their maximum strength is presently modest and experimental aerodynamic applications so far have been generally limited in speed and Reynolds number to about 10–30 m/s and 10^4–10^5, respectively. Consequently, this first study of concept is being performed for a small wing of 6 in. in chord at an incoming air speed of 15 m/s, corresponding to a Reynolds number of about 150,000, which is in the range associated with radio-controlled airplanes or small UAVs. However, plasma actuation strength has been growing rapidly, and should this concept show promise, further CFD simulations will allow estimation of the actuation strength required under speeds and Reynolds numbers associated with larger aircraft.

The next section describes the methodology, starting with the wing geometry, followed by the computational approach including the plasma actuator model and its implementation in the CFD code, and ending with the experimental setup. Subsequently, the results of the simulations are shown and discussed, followed by experimental results to support the predictions, and ending with preliminary results for lift generation on a symmetric wing. Finally, the conclusions of the present work are summarized.

II. Methodology

A. Geometry Selection

For this first study of the proposed concept, the wing geometry is selected based on simplicity and the ability to be tested in a subsonic wind-tunnel test section of $0.61 \times 0.61 \times 2.44$ m ($24 \times 24 \times 96$ in.) in size, to have experimental data to support the findings of the simulations. The chosen geometry is a two-dimensional (half) wing with a semicircular rounded tip, and with a chord of 15.24 cm (6 in.) and a span (including tip) of 31.88 cm (12.55 in.) to have a reasonable aspect ratio while fitting in the test section. It is designed to be installed vertically at zero angle of attack in the wind-tunnel test section (Fig. 3) on an aerodynamic balance installed under the test section to measure aerodynamic moment. A NACA 4418 cross section is selected to give enough thickness to install a plasma actuator on the rounded tip surface, if needed, while being reasonably thin to minimize negative effects on the nominal lift from the tunnel walls. Figure 4 shows the wing geometry with the placement, set by the available space on the experimental wing, of the plasma actuators on the upper/lower surfaces as well as on the wing tip. The actuators on the suction and pressure sides extends from 10% chord to the trailing edge, and their position, defined by the location of the center of the gap between the exposed and hidden electrodes, is at 91% span. Most simulations and the experiments carried out so far only include these two actuators. A simulation is also carried out with an actuator on the wing tip extending from 10 to 78% chord.

B. Actuator Model

A model of the DBD actuator is needed to carry out CFD simulations of the concept. In the past few years, many models have been developed, with varying complexity, to simulate the fluid

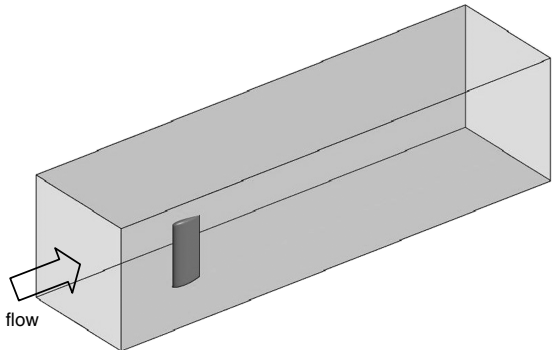

Fig. 3 Wing test configuration in wind-tunnel section.

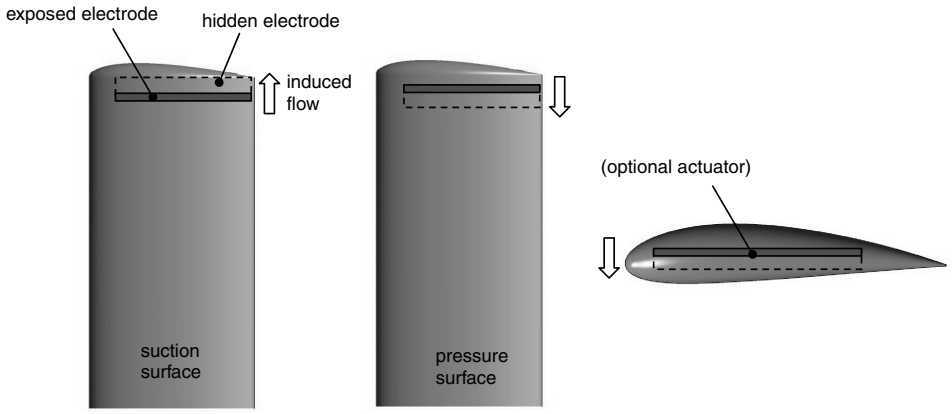

Fig. 4 Wing geometry and plasma actuator locations.

dynamic effect of plasma actuators. The simplest models replace the actuator with a doublet [20] for incorporation into a panel method code for flow around an airfoil or represent the plasma–fluid dynamics coupling in one dimension with an electrostatic body force [21] based on charge density. Shyy et al. [22] proposed a more sophisticated, yet simple, model that provides a time-averaged linear two-dimensional body-force distribution in terms of the actuator size and input voltage amplitude and frequency. Suzen et al. [23] developed a model that produces a more realistic body-force distribution based on actuator geometry and the nature of the fluid and dielectric material. This body-force distribution is then modulated in time with the alternating voltage input. Orlov et al. [24] used a network of electrical elements to model the dynamics of the glow discharge (plasma) region over the encapsulated (hidden) electrode to obtain a more accurate spatial and time variation of the induced body force. Finally, the most sophisticated models [25–27] couple the equations governing the motion of ions and electrons to the flow equations. However, these models are too costly in computational time and resources to be used directly in applied aerodynamics CFD simulations at the macroscale level.

Among the models cited above, the time-averaged spatial body-force distribution approach provides the most effective modelling of plasma actuation for flow control in complex flow problems. According to Orlov et al. [28], the time scales associated with the ionization and with the ac input cycle of the actuator are six and two orders of magnitude, respectively, faster than the response of the flow. The plasma formation process is thus quasi-instantaneous from the point of view of the flow, thus allowing for the use of a time-averaged body-force distribution that captures the net spatial effect of the actuation on the flow near surface boundaries, without adding significant computational cost. This is the approach taken in most numerical flow control studies with plasma actuator. Indeed, even an approximate time-averaged linear spatial force distribution as proposed by Shyy et al. [22] can generate an induced-velocity profile shape that resembles the experimental profile. However, there has yet to be a validated model giving an accurate time-varying body force with respect to actuator geometry and input. Thus, the proposed approach in this study consists of using the most accurate representative time–averaged spatial body-force distribution possible that is achievable with a low-cost model and scaling it to obtain the desired total (integrated) induced body force. This total body force is henceforth referred to as the actuator strength and is given per unit length of actuator (mN/m). The model chosen in the present study is a new hybrid model by Lemire and Vo [29] that combines the best features of the models by Suzen et al. [23] and Orlov and Corke [24] to give a body-force distribution, as shown in Fig. 5, which resembles that obtained with one of the much more sophisticated models [27]. This body-force distribution, which is obtained by solving the model equations [29] on a very fine rectangular mesh, is mapped onto the coarser CFD mesh of the arbitrarily curved aerodynamic surface on which the plasma actuator is placed using the method outlined by Lemire and Vo [29]. The vectors are then scaled to obtain the desired total induced body-force (actuator strength) value.

C. Computational Setup

Two computational studies are in fact carried out for the NACA 4418 wing. The first is a very preliminary study using the Reynolds-averaged Navier–Stokes CFD code UNSTREST [30] from the University of Cambridge to justify investing into developing more accurate simulations and an experimental setup. UNSTREST is a time-accurate turbomachinery CFD code, which had been modified to implement body-force-type plasma actuator models and had already been used for several studies of plasma actuation in compressors [7,29]. Because of the nature of the code, the geometry of the computational domain shown in Figs. 3 and 4 can only be approximated. The cantilevered wing is modeled as one of many identical zero-stagger blades in a stator row with a large 3 m (118 in.) hub radius and 3.6 m (142 in.) shroud radius, as shown in Fig. 6a. A pinched tip is used, giving an almost rounded tip in the region near the thickest part of the airfoil, as shown in Fig. 6b, but not necessarily along the entire chord. In this early study, a 0.3126 m (12.31 in.) span is simulated, with the actuators placed closer to the wing tip (95% and 98% span for the suction- and pressure-side actuators, respectively). A structured mesh with 862,000 nodes is used per blade passage with higher mesh density near the blade surface and in the tip region. The airfoil design code XFOIL [31] is used to determine the transition point on the upper and lower surfaces and input into UNSTREST, with a mixing-length turbulence model and a wall function used downstream of this point. Uniform stagnation pressure and temperature at atmospheric conditions and axial flow are assigned as boundary conditions at the domain inlet and a uniform static pressure value is imposed at the domain exit to give the desired inlet velocity of 15 m/s. The simulations with UNSTREST only incorporated the actuators on the suction and pressure sides, modeled as the mapped body-force distributions shown in Fig. 6b. The lift is obtained from summing the pressure forces over the blade during postprocessing in MATLAB.

Following encouraging results from the simulations with UNSTREST, the main and more accurate computational study is carried out using ANSYS CFX 11, with a shear stress transport turbulence model and a $\gamma - \theta$ boundary-layer transition model. A user-defined function is written to implement the spatial force distribution (representing the plasma actuator) in CFX. The fluid domain incorporating the wing within the wind-tunnel test section, as shown in Figs. 3 and 4 is meshed with GAMBIT. It is divided into subdomains as illustrated in Fig. 7a to allow for a structured mesh, shown in Fig. 7b, in order to facilitate mapping and implementation of the spatial body-force distributions. The computational domain has 507,400 nodes. Although the mesh density is increased in the same regions as with UNSTREST, a wall function is not used and the first mesh above the wing surfaces is therefore set to have $y^+ < 1$ as required by the transition model. The boundary-layer simulation by CFX 11 has been checked in terms of transition location with XFOIL and of the separation point through comparison with experimental data [32] for a NACA 0018 airfoil. The boundary conditions at the domain inlet consisted of uniform distributions of total pressure, total temperature at atmospheric conditions and an imposed velocity that is axial and 15 m/s in magnitude. The simulations are carried out in

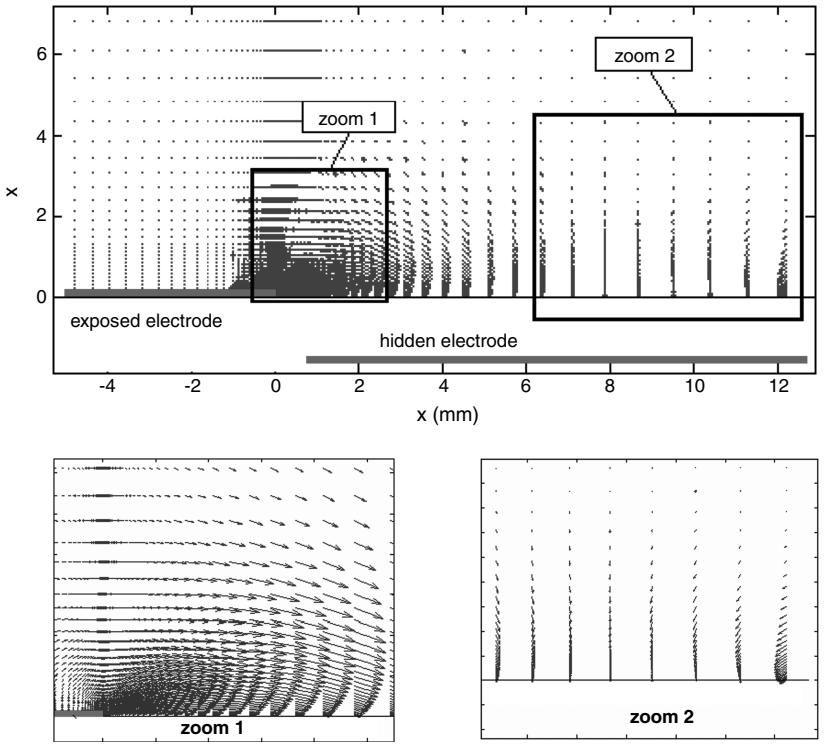

Fig. 5 Plasma actuator body-force distribution.

steady mode. The lift and drag are obtained using the associated standard functions in CFX.

D. Experimental Setup

Wind-tunnel experiments are carried out to provide preliminary test data against which to verify the predictions by CFD for the low end of the actuator strength range, on the order of the strength of the tested actuators. The subsonic closed-loop wind-tunnel manufactured by ELD, Inc., (model 407B) possesses a rectangular test section of $0.61 \times 0.61 \times 2.44$ m and is capable of air speeds up to 91 m/s. The wing is placed inside the test section as illustrated in Fig. 3. A small Pitot tube is placed in the flow upstream and away from the wing to measure the incoming flow velocity. The wing is connected to an L-shaped balance system (Fig. 8) that allows measurement of the aerodynamic moment by the change in force exerted on the electronic scale, the distance between the scale and support can be varied to increase the force exerted on the scale and thus increase measurement resolution. The pivot of the balance consists of a hollow tube mounted on a set of ball bearings through which the

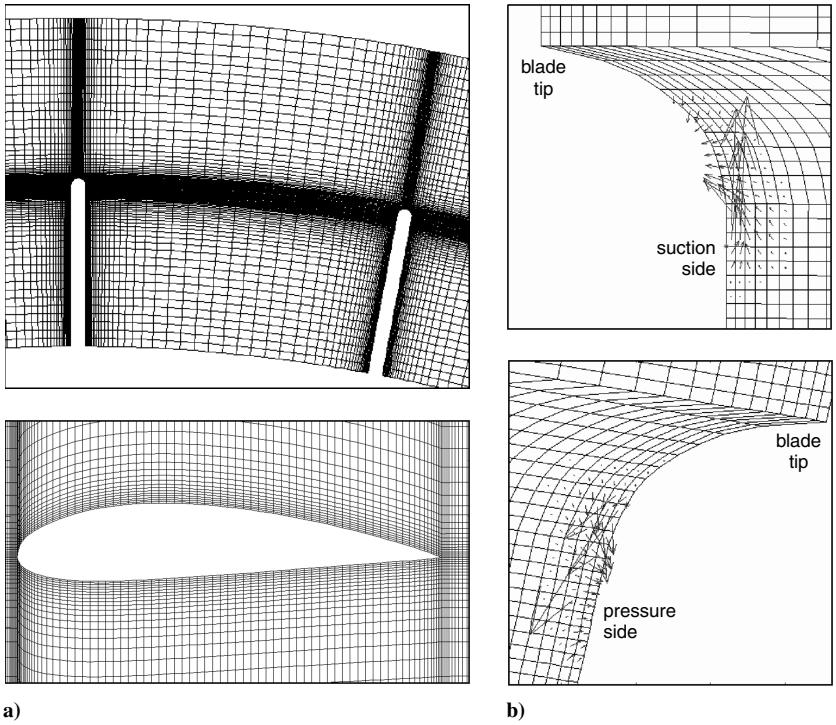

Fig. 6 UNSTREST a) computational domain and b) plasma actuation model.

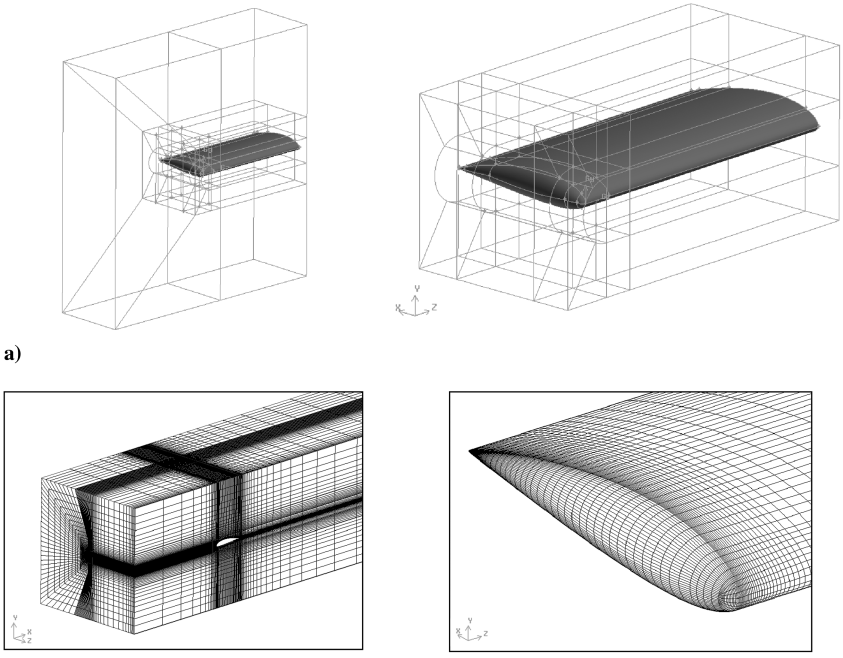

Fig. 7 CFX a) computational domain subdivisions and b) structured mesh.

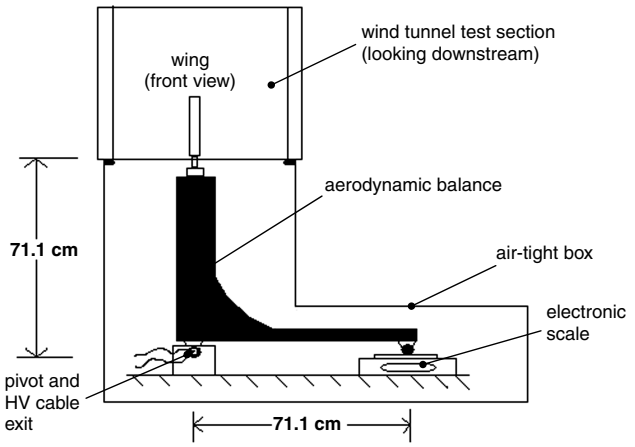

Fig. 8 Aerodynamic balance system for measuring aerodynamic moment.

high-voltage actuator wires come out, to minimize to negligible levels any effect of the wires on the measured moment. The electronic scale can thus be located far enough from the high-voltage wires to avoid electromagnetic interference. The entire setup is placed inside an airtight box within which the pressure is equal to the static pressure of the wind-tunnel test section. A window on the box allows reading of the electronic scale.

The wing is made from balsa wood and covered with a plastic coating used for radio-controlled aircraft. A metal tube serves as the main spar (and connection to the balance) in which run the input cables to the actuators. The actuators are made with 0.076-mm-thick tinfoil tape for the electrodes separated by a 0.305-mm-thick dielectric made of layers of self-adhering Kapton tape (two layers at 0.127 mm thick and one at 0.051 mm thick). The exposed and hidden electrodes are 3 and 12.7 mm wide, respectively, with a zero axial gap between them. The dielectric is mounted approximately flush with the wing surface. This traditional configuration of plasma actuator has been shown to give actuator strengths between 20 and 40 mN/m, depending on the exact size of the electrodes and dielectric, the axial offset between electrodes, and atmospheric conditions (humidity, etc.). It must be noted that these experiments are meant as a preliminary order-of-magnitude verification of the computationally predicted forces with available actuators rather than an exact validation of the computational results. Consequently, the exact match between experiments and simulations, especially in terms of the actuator strength, is not necessary in the context of this study.

The plasma actuators are driven by a Minipuls2 high-voltage generator from ElectroFluid Systems with a 160 W, 0–25 kV peak-to-peak, 5–30 kHz capability. All actuators are actuated in phase with a sinusoidal input from the generator set at 15.3 kV peak-to-peak (the highest reachable value for the present actuator setup) and 7 kHz to get the highest plasma density (optimized actuator strength). The experimental procedure consists of saving the reading of the electronic scale at zero incoming velocity and recording the change in this reading at a desired air speed to deduce the moment without actuation and repeating this measurement with the actuator turned on to calculate the change in moment due to the actuators.

III. Results and Discussion

In the past few years, published actuator strengths have grown by an order of magnitude [33] and thus actuator strengths on the order of several newtons/meter can be expected in the near future for the next generation of actuators with improved and optimized configurations [28] and new input technologies such as nanopulsing [34]. This study therefore considers actuator strengths of 40 mN/m (the best that can be achieved with traditional DBD actuators), 200 mN/m (achievable with the most recent actuators [35]), and 400 mN/m (considered to be achievable in the short term).

Table 1 summarizes the results from the preliminary computational study with UNSTREST using the approximated geometry of Fig. 6 with actuators on the pressure and suction sides only. They indicate an approximately linear increase in lift (same as variation in

Table 1 Results from preliminary simulations with UNSTREST with actuators on pressure and suction sides

Case number	Actuator strength, mN/m	C_L	Change in lift, %
01	0	0.2448	——
02	40	0.2485	1.50
03	200	0.2625	7.23
04	400	0.2740	11.90

lift coefficient C_L) with actuation strength, starting from what should be experimentally measurable levels at 40 mN/m, and reaching interesting levels for roll control at higher actuator strengths, even with only two actuators.

The results from the more detailed and accurate computational study with the intended geometry of Figs. 3, 4, and 7 using ANSYS CFX 11 are shown in the subsequent tables and figures. Table 2 summarizes the main simulations carried out in CFX for actuation

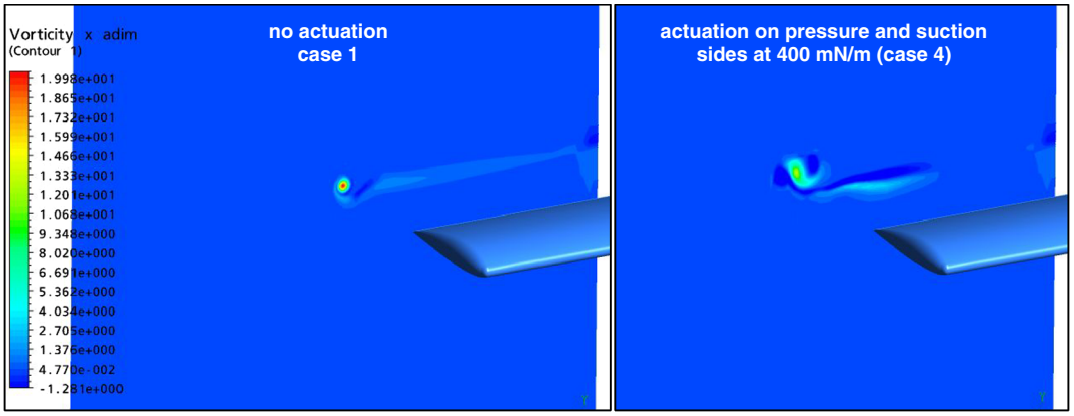

Fig. 9 Nondimensional (streamwise) vorticity contours one chord downstream of trailing edge without and with pressure- and suction-side actuation.

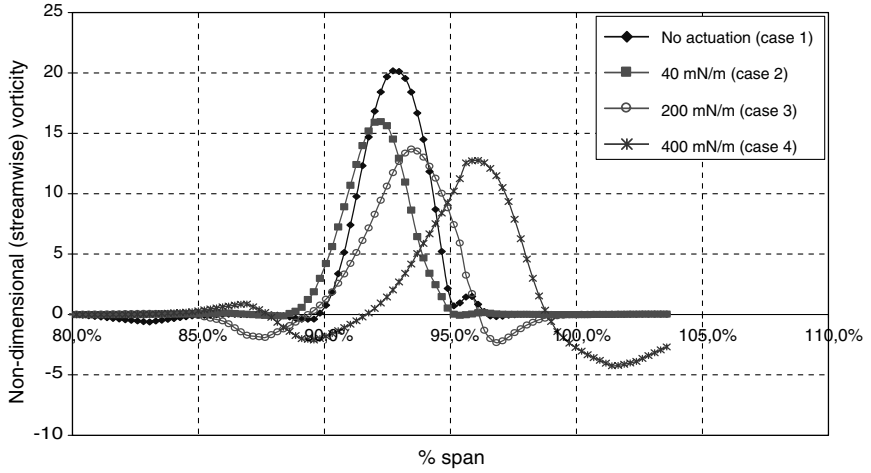

Fig. 10 Nondimensional (streamwise) vorticity versus span for spanwise line through tip vortex center line at one chord downstream of trailing edge for different pressure and suction sides actuator strength.

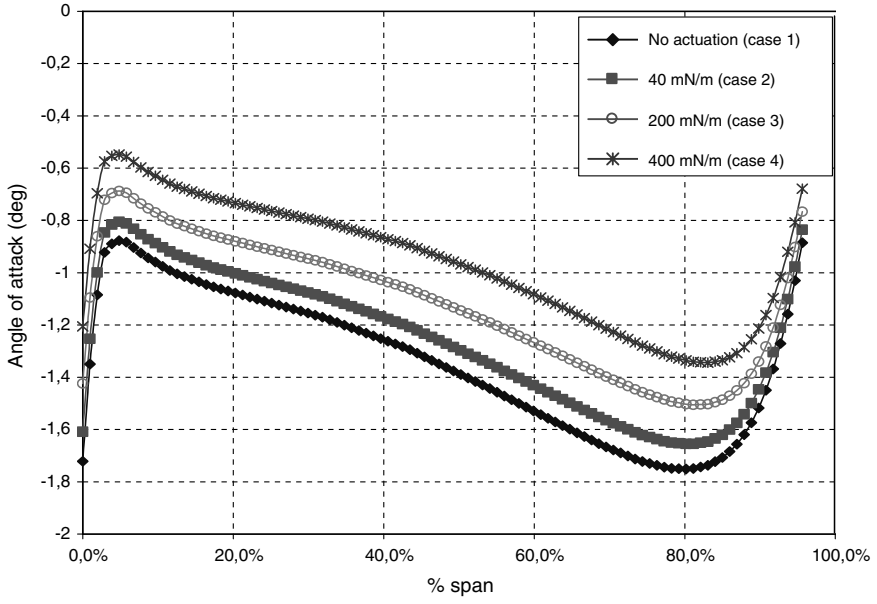

Fig. 11 Effect of pressure- and suction-side actuation strength on angle of attack at 10% chord upstream of leading edge.

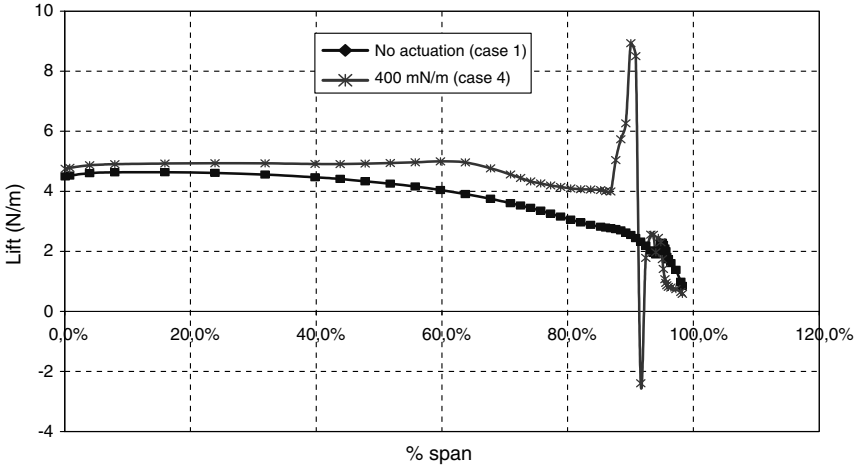

Fig. 12 Effect of pressure- and suction-side actuation spanwise lift distribution.

opposing the tip vortex. There is a little difference in the predicted C_L and in increases in lift of cases 1 through 4 with those of the preliminary study (cases 01 though 04 in Table 1) that could be due to the difference in codes, mesh, turbulence models, and computational geometry, and exact actuator location. However, the match in order of magnitude and in trend between the two different computational studies further reinforces the validity of the predictions. The simulation cases 4 through 6 indicate that the total effect on lift is the sum of the effect of each actuator, with the actuator on the suction side contributing about 3 times more to lift increase than the one on the pressure side. For case 7, an actuator is placed on the semicircular wing tip, as shown in Fig. 4. However, due to problems with body-force mapping onto this highly curved surface, only the main body-force vectors were transferred causing the integral body force

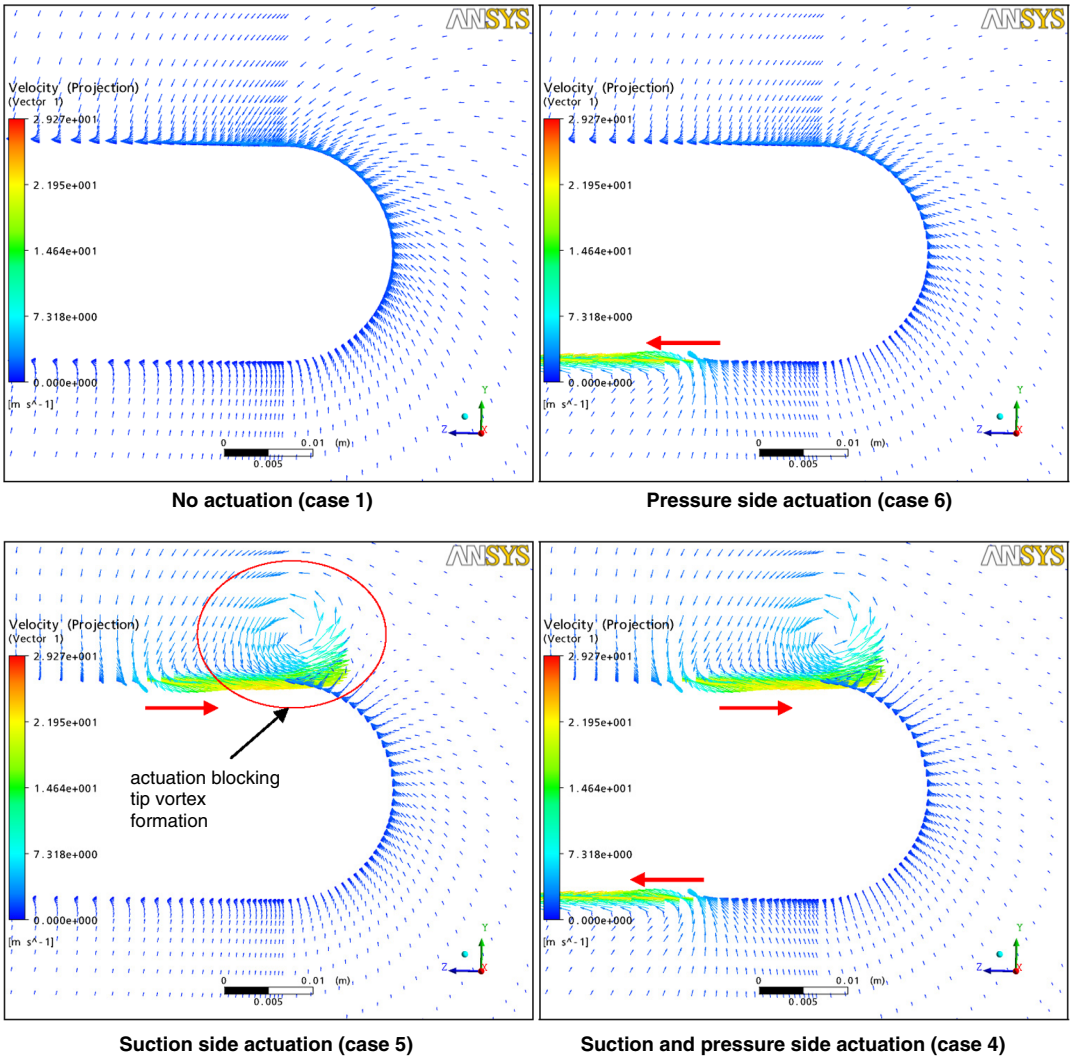

Fig. 13 Transverse velocity vectors at midchord for different actuation configurations.

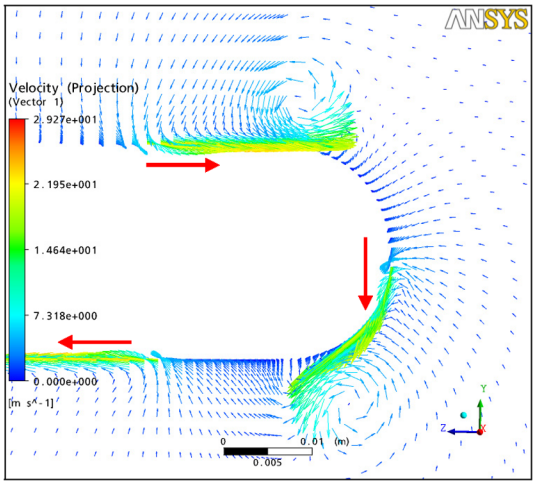

Fig. 14 Transverse velocity vectors at midchord with pressure side, suction side, and tip actuators (case 7).

to be about 75% of that of pressure- and suction-side actuators. Even then, with 400 mN/m, the increase in lift is almost 20%. Finally, the lift augmentation is accompanied by a modest increase in drag.

The next part of the discussion focuses on the source of the increase in lift and drag. The first aspect to investigate is the tip vortex. Figure 9 shows the contours of axial (streamwise) vorticity, nondimensionalized by the incoming velocity over the chord, on a plane one chord downstream of the trailing edge, for the reference case (case 1) and with 400 mN/m pressure/suction-side actuation (case 4). Comparison of the two cases indicates that although the total circulation of the tip vortex has not decreased, the vortex core is more diffused, with a larger diameter and lower vorticity distribution as a result of the actuation. This is also evident in Fig. 10, which shows the streamwise vorticity for a line through the tip vortex center that is parallel to the wing span at one chord downstream of the trailing edge for cases 1 through 4. It is clear from this figure that the vortex core intensity is reduced as the actuation strength is increased, but also that the vortex core moves further outward, although only for the higher actuator strengths. Furthermore Figs. 9 and 10 also show that the wing-tip plasma actuation has created two regions of negative vorticity around the tip vortex. All three of these effects reduce the downwash caused by the tip vortex and are thus beneficial to the wing lift. Moreover, the fact that 40 mN/m actuation (case 2) results in lift increase even though the tip vortex has actually moved inboard (see Fig. 10) indicates that outboard tip vortex displacement is not the only mechanism contributing to lift improvement. As expected, Fig. 11 points to an increasing alleviation of the negative angle of attack induced by the downwash from the tip vortex with rising actuation strength for cases 1 through 4. The benefit is observed in the increased and more uniform spanwise lift distribution for case 4 versus case 1 in Fig. 12.

Figure 13 illustrates the mechanism by which each of the suction- and pressure-side actuators contribute to weakening the tip vortex with plots of the transverse flow field in the blade tip region at the midchord. Case 1 illustrates the flow around the wing tip from the pressure side toward the suction side that is at the origin of the tip vortex formation. Case 5 shows that the outward-induced jet from the suction-side actuator effectively blocks the flow around the wing tip, markedly reducing it. For case 6, inward injection toward the wing root on the pressure side relies on viscous flow induction to slow down the flow around the wing tip, which it succeeds to do, but this method is less effective than suction-side outward-induced flow. The combination of both actuators (case 4) adds up the effects. Figure 14 illustrates the effect of the addition of the wing-tip actuator (case 7) whose downward induced jet forms an additional barrier against the flow from the suction side.

Although the reduced tip vortex intensity should have entrained a reduction in drag (from a drop in induced drag), the results show a modest increase in drag. This increase can be explained by looking at the shear stress distribution on the wing surface, as plotted for the suction side of case 5 in Fig. 15, which exhibits an increase in the region of the induced spanwise jet from the actuator. Indeed, the actuation induces additional turbulence in this region, resulting in higher surface shear. This added turbulence and higher shear is also evident from the much fuller streamwise velocity profile in the suction-side boundary layer in the tip region for case 5 versus case 1, as shown in Fig. 16. Although not shown, the same observation applies to the plasma actuation on the pressure side.

Figure 17 presents the experimentally measured increase in moment with the setup shown in Fig. 8 for pressure- and suction-side actuation (comparable to case 2 in Table 2) for a constant actuator strength at different incoming velocities. Three similar sets of runs are carried out, with representative error bars placed on one set. The error bars are based on measurement uncertainty from the accuracy of the electronic scale and oscillations in the readings observed during the tests. Since the actual strength of this type of Kapton DBD actuator is usually in the 20–30 mN/m range, corresponding CFX simulations at 25 mN/m actuator strength are carried out in advance for comparison. For reasons related to the construction of the experimental wing, its span had to be 20% longer than the simulated wing. Since the CFD simulations show that the spanwise lift distribution at the wing root is virtually constant and unaffected by a 25 mN/m actuation, the CFD results were appropriately corrected to account for the difference in wing spans. The resulting predicted moments are plotted in Fig. 17 along with the experimental data. Two observations can be made. First, there is an order-of-magnitude agreement in the predicted change in moment from the actuation. The experimental values are smaller than the CFD prediction. The most likely reason could be that the wing-tip leading edge of the

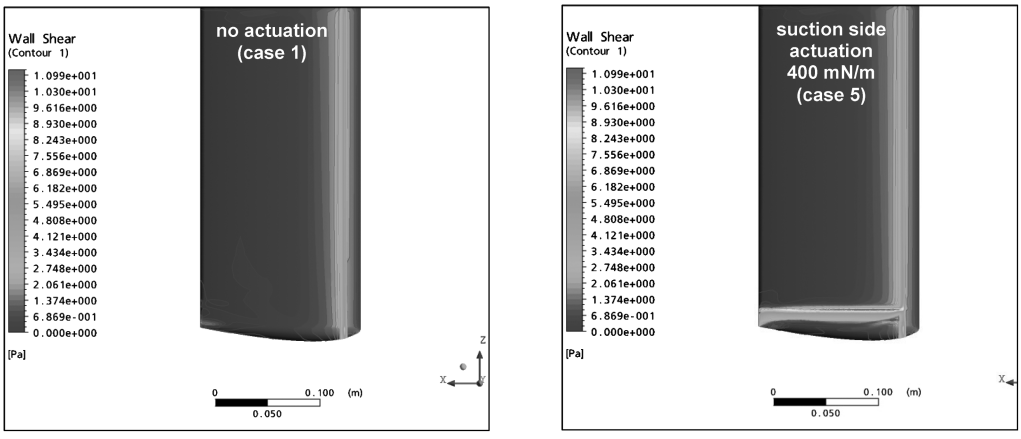

Fig. 15 Effect of actuation on shear stress distribution on the suction surface.

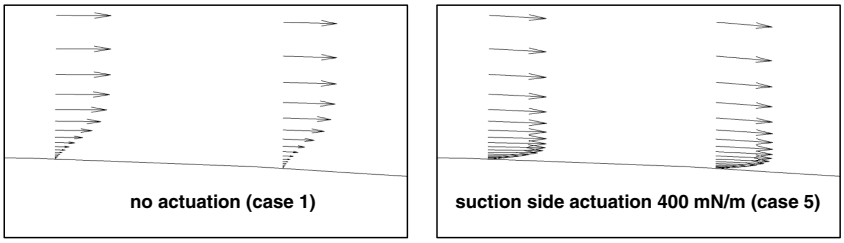

Fig. 16 Streamwise velocity profile on suction surface at midchord and 93% span.

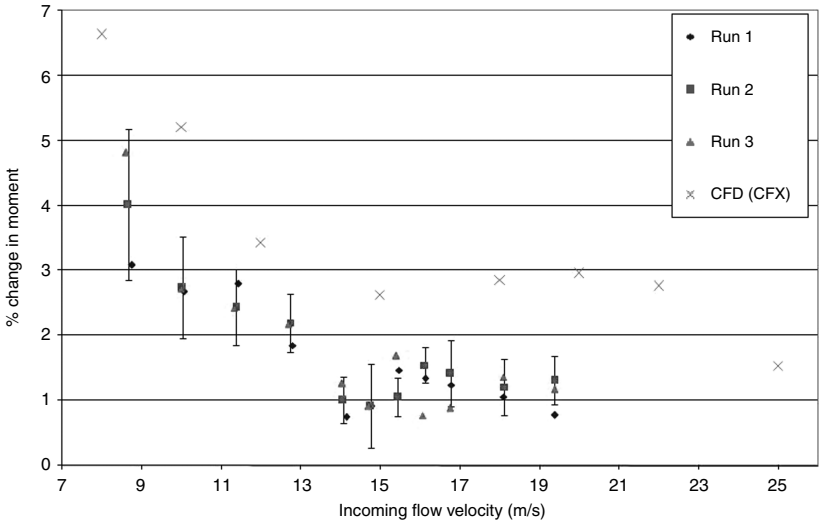

Fig. 17 Increase in lift versus incoming air speed at the lowest actuation strength.

experimental wing has a 4 mm protrusion from the two high-voltage wires connected to the exposed electrodes, which may affect the aerodynamics in the tip region.

The second observation is the match between experiments and CFD predictions of the peculiar trend of lift increase versus incoming flow velocity. Moreover, this trend shows a local minimum at 15 m/s, which implies even better performance of the concept at other velocities for the same actuator strength.

Although done only for limited actuation strength, the experimental results add further support for the CFD predictions and by extension for the simulated performance of the proposed concept at higher actuation strengths.

Finally, preliminary simulations in ANSYS CFX 11 are carried out to assess the capability of the proposed actuation concept to generate lift on a non lifting surface. A low-aspect ratio symmetric wing (a reasonable representation of a tail surface) is simulated at zero angle of attack. A larger wing with a 20.96 cm (8.25 in.) chord and a 43.79 cm (17.24 in.) span using a NACA 0018 cross-section is chosen to be mounted horizontally in the wind-tunnel test section, as shown in Fig. 18, which also illustrates the upper and lower plasma actuators at 78% span (from the midspan symmetry line) and extending from 7 to 90% chord, while the actuators on the round wing tips extend from 7 to 78% chord. For the wing-tip actuator, as in the case of the NACA 4418 wing, only the main body-force vectors were modeled causing the integral body force to be also about 75% of that of pressure- and suction-side actuators. Because of the symmetry, a half wing span and fluid domain is simulated. The mesh has 505,661 nodes. The results, summarized in Table 3, show an increased lift generation with increasing actuation strength and indicate that the generated lift is the sum of the effect of each actuator. However, the total generated lift only becomes important relative to drag at large actuator strengths. Preliminary investigation into the source of lift generation indicates a dramatic effect of the actuation on the flow field at the symmetric wing tip. Figure 19 shows the contours of axial (streamwise) vorticity, nondimensionalized by the incoming velocity over the chord, on a plane one chord downstream of the trailing edge. The reference case (case 11), and the case with 40 mN/m actuators on the pressure/suction sides and wing tip (at 30 mN/m) (case 16) are shown. In the reference case, there are two symmetric small counter-rotating tip vortices. However, the actuation creates an asymmetrical network of multiple counter-rotating vortical structures in the outer span, whose combined influence

Table 2 Results from CFX simulations for actuation against the tip vortex

Case number	Actuator locations	Actuator strength, mN/m	C_L	Change in lift, %	C_D	Change in drag, %
1	No actuation	0	0.1931	——	0.0255	——
2	Pressure and suction sides	40	0.1994	3.27	0.0257	0.75
3	Pressure and suction sides	200	0.2114	9.49	0.0261	2.22
4	Pressure and suction sides	400	0.2247	16.36	0.0265	3.80
5	Suction side only	400	0.2172	12.48	0.0262	2.71
6	Pressure side only	400	0.2009	4.01	0.0259	1.35
7	Pressure and suction sides And wing tip	400	0.2307	19.48	0.0269	5.40

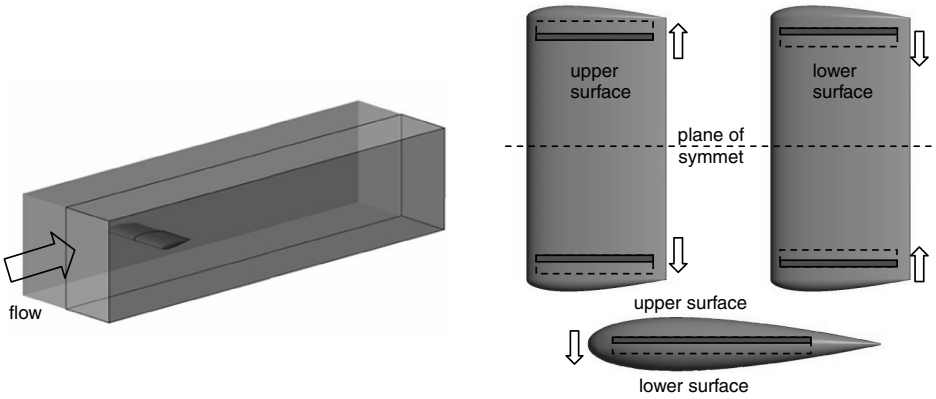

Fig. 18 Symmetric NACA 0018 wing and plasma actuator locations.

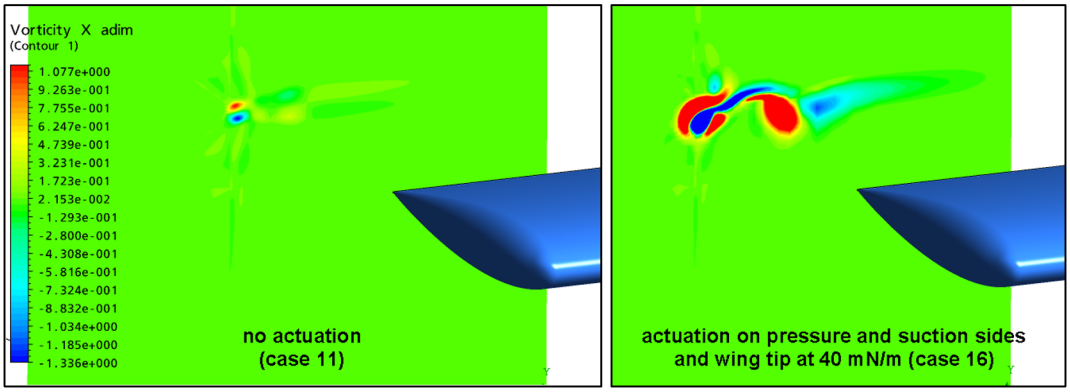

Fig. 19 Nondimensional vorticity contours one chord downstream of the trailing edge on a NACA0018 wing without and with pressure- and suction-side actuation.

generates lift on the symmetric wing. Further analysis is needed to investigate more closely the results from this extension of the proposed concept and is beyond the scope of this paper.

IV. Conclusions

A computational and preliminary experimental study is carried out on a small NACA 4418 wing with a rounded tip at Reynolds numbers on the order of 150,000 to evaluate the concept of wing-tip plasma actuation to alter lift for roll control at low angles of attack by affecting the tip vortex in the context of vorticity distribution downstream of the trailing edge. CFD simulations with ANSYS CFX show a noticeable increase in lift, even at small actuation strength of 40 mN/m, associated with conventional DBD actuators. This increase in lift reaches almost 20% for an actuation strength of 400 mN/m, likely achievable in the short term. The largest contribution to lift improvement comes from the suction-side actuator whose outward spanwise induced jet blocks the flow around the blade tip that forms the tip vortex. The markedly smaller contribution from the inward-pointing pressure-side actuator is almost linearly added to obtain the total effect. The downward-pointing tip actuator adds a further small contribution to the lift increase. The lift augmentation results from alteration of the streamwise vorticity distribution downstream of the trailing edge that results in a more diffused tip vortex surrounded by negative vorticity induced by the actuators and, but not necessarily, outboard displacement of the tip vortex. These factors reduce the downwash upstream of the wing and consequently increase its lift. A modest increase in drag is also associated with the increase in lift, due to larger surface shear stress levels near the actuator. A preliminary computational study with a completely different CFD code and an approximated geometry show similar changes in lift. Furthermore, wind-tunnel experiments with low actuator strength also support the lift increase results of the CFD study in magnitude and trend. Overall, the results are very promising and encourage further research into this concept for flow control, which should focus on two aspects. The first is the effect of change in angle of attack on the change in lift for the same actuator strength. However, only a relatively small range of angles of attack needs to be covered, since at higher angles where the suction-side boundary layer nears separation, plasma actuation directed streamwise on the

Table 3 Results from CFX simulations for symmetric NACA 0018 wing

Case number	Actuator locations (reversed actuation)	Actuator strength, mN/m	C_L	C_D	Change in drag, %
11	No actuation	0	−0.0002	0.0128	——
12	Upper surface only	40	0.0041	0.0130	2.04
13	Lower surface only	40	0.0077	0.0131	2.69
14	Wing tip only	40	0.0017	0.0131	2.46
15	Upper and lower surfaces	40	0.0116	0.0134	4.73
16	Upper and lower surfaces and wing tip	40	0.0123	0.0136	6.70
17	Upper and lower surfaces and wing tip	200	0.0285	0.0152	18.86
18	Upper and lower surfaces and wing tip	400	0.0358	0.0166	30.11

suction side may be more effective in altering lift. The second aspect to investigate in future studies is the effectiveness of the proposed concept and the actuation strength required for higher Reynolds numbers associated with full-scale aircraft.

Preliminary computational simulations are carried out to evaluate the generation of lift with the same proposed concept on a symmetrical wing to simulate a tail surface for pitch and yaw control. The results do show lift generation increasing with actuator strength, becoming larger than drag only at higher actuator strengths. Further investigations need to be carried out into this extension of the proposed actuation concept.

Acknowledgments

The authors are grateful to the Natural Sciences and Engineering Research Council of Canada (NSERC), whose funding under the Discovery Grants program was used to carry out this work. The authors would like to thank Sébastien Lemire and Xiaofei Xu for their help in implementing the actuator model in the computational fluid dynamics code, as well as Jonathan Doré, Vincent Labrèche, and Philippe Versailles for their roles in the design and fabrication of the experimental setup.

References

[1] Enloe, C. L., McLaughlin, T. E., Van Dyken, R. D., Kachner, K. D., Jumper, E. J., and Corke, T., "Mechanisms and Responses of a Single Dielectric Barrier Plasma Actuator: Plasma Morphology," *AIAA Journal*, Vol. 42, No. 3, 2004, pp. 589–594. doi:10.2514/1.2305

[2] Corke, T., and Post, M., "Overview of Plasma Flow Control: Concepts, Optimization, and Applications," AIAA Paper 2005-563, 2005.

[3] Goeksel, B., Rechenberg, I., Greenblatt, D., and Paschereit, C. O., "Steady and Unsteady Plasma Wall Jets for Separation and Circulation Control," AIAA Paper 2006-3686, 2006.

[4] Huang, J., Corke, T. C., and Thomas, F., "Plasma Actuators for Separation Control of Low Pressure Turbine Blades," AIAA Paper 2003-1027, 2003.

[5] Boxx, I. G., Newcamp, J. M., Franke, M. E., Woods, N. M., and Rivir, R. B., "A PIV Study of a Plasma Discharge Flow-Control Actuator on a Flat Plate in an Aggressive Pressure Induced Separation," American Society of Mechanical Engineers, Paper GT2006-91044, 2006.

[6] Morris, S., Corke, T., VanNess, D., Stephens, J., and Douville, T., "Tip Clearance Control Using Plasma Actuator," AIAA Paper 2005-782, 2005.

[7] Vo, H. D., "Suppression of Short Length-scale Rotating Stall Inception with Glow Discharge," American Society of Mechanical Engineers, Paper GT2007-27673, 2007.

[8] Nelson, R., Corke, T., He, C., Othman, H., Matsuno, T., Patel, M., and Ng, T., "Modification of the Flow Structure over a UAV Wing for Roll Control," AIAA Paper 2007-884, 2007.

[9] Lopera, J., Ng, T., Patel, M., Vasudevan, S., and Corke, T., "Aerodynamic Control of 1303 UAV Using Windward Surface Plasma Actuators on a Separation Ramp," AIAA Paper 2007-636, 2007.

[10] Ayers, R. F., and Wilde, M. R., "An Experimental Investigation of the Aerodynamic Characteristics of a Low Aspect Ratio Swept Wing with Blowing in a Spanwise Direction from the Tips," College of Aeronautics, Note 57, Cranfield, England, U.K., Sept. 1956.

[11] White, H. E., "Wind-Tunnel Investigation of the Use of Wing Tip Blowing to Reduce Drag for Take-Off and Landing," David Taylor Model Basin Aerodynamics Lab., AERO Rept. 1043, Washington, D.C., 1963.

[12] Wu, J. M., Vakili, A. D., and Gilliam, F. T., "Aerodynamic Interaction of Wing Tip Flow with Discrete Wing Tip Jets," AIAA Paper 84-2206, 1984.

[13] Tavella, D., Wood, N., Lee, C. S., and Roberts, L., "Lift Modulation with Lateral Wing-Tip Blowing," *Journal of Aircraft*, Vol. 25, No. 4, 1988, pp. 311–316. doi:10.2514/3.45565

[14] Simpson, R. G., Ahmed, N. A., and Archer, R. D., "Near Field Study of Vortex Attenuation Using Wing-Tip Blowing," *The Aeronautical Journal*, Vol. 106, No. 1057, 2002, pp. 117–120.

[15] Duraisamy, K., and Baeder, J. D., "Numerical Simulation of the Effects of Spanwise Blowing on Wing-Tip Vortex Formation and Evolution," AIAA Paper 2005-4726, 2005.

[16] Okada, S., and Hiraoka, K., "Experimental Studies of Reduction of the Wing Tip Vortex by Suction," AIAA Paper 2003-3533, 2003.

[17] Margaris, P., and Gursul, I., "Wing Tip Vortex Control Using Synthetic Jets," *The Aeronautical Journal*, Vol. 110, No. 1112, 2006, pp. 673–681.

[18] Ramakumar, K., and Jacob, J. D., "Flow Control and Lift Enhancement Using Plasma Actuators," AIAA Paper 2005-4635, 2005.

[19] Santhanakrishnan, A., Pern, N. J., Ramakumar, K., Simpson, A., and Jacob, J. D., "Enabling Flow Control Technology for Low Speed UAVs," AIAA Paper 2005-6960, 2005.

[20] Hall, K. D., Jumper, E. J., Corke, T. C., and McLaughlin, T. E., "Potential Flow Model of a Plasma Actuator as a Lift Enhancement Device," AIAA Paper 2005-783, 2005.

[21] Roth, J. R., "Aerodynamic flow Acceleration Using Paraelectric and Peristaltic Electrohydrodynamic Effects of a One Atmosphere Uniform Glow Discharge Plasma," *Physics of Plasmas*, Vol. 10, No. 5, 2003, pp. 2117–2126. doi:10.1063/1.1564823

[22] Shyy, W., Jayaraman, B., and Andersson, A., "Modeling of Glow Discharge-Induced Fluid Dynamics," *Journal of Applied Physics*, Vol. 92, No. 11, 2002, pp. 6434–6443. doi:10.1063/1.1515103

[23] Suzen, Y. B., Huang, P. G., Jacob, J. D., and Ashpis, D. E., "Numerical Simulations of Plasma Based Flow Control Applications," AIAA Paper 2005-4633, 2005.

[24] Orlov, D. M., and Corke, T. C., "Electric Circuit Model for Aerodynamic Plasma Actuator," AIAA Paper 2006-1206, 2006.

[25] Roy, S., Singh, K. P., Kumar, H., Gaitonde, D. V., and Visbal, M. R., "Effective Discharge Dynamics for Plasma Actuators," AIAA Paper 2006-374, 2006.

[26] Jayaraman, B., Thakur, S., and Shyy, W., "Modeling of Dielectric Barrier Discharge and Resulting Fluid Dynamics," AIAA Paper 2006-686, 2006.

[27] Gaitonde, D. V., Visbal, M. R., and Roy, S., "A Coupled Approach for Plasma-Based Flow Control Simulations of Wing Sections," AIAA Paper 2006-1205, 2006.

[28] Orlov, D. M., Apker, T., He, C., Othman, H., and Corke, T., "Modeling and Experiment of Leading Edge Separation Control Using SDBD Plasma Actuators," AIAA Paper 2007-0877, 2007.

[29] Lemire, S., and Vo, H. D., "Reduction of Fan and Compressor Wake Defect Using Plasma Actuation for Tonal Noise Reduction," Accepted for publication in Journal of Turbomachinery, American Society of Mechanical Engineers, Paper GT2007-50821, 2008.

[30] Denton, J. D., "The Use of a Distributed Body Force to Simulate Viscous Effects in 3D Flow Calculations," American Society of Mechanical Engineers, Paper 86-GT-144, 1986.

[31] Drela, M., and Giles, M. B., "Viscous-Inviscid Analysis of Transonic and Low Reynolds Number Airfoils," *AIAA Journal*, Vol. 25, No. 10, 1987, pp. 1347–1355. doi:10.2514/3.9789

[32] Nakano, T., Fujisawa, N., Oguma, Y., Takagi, Y., and Lee, S., "Experimental Study on Flow and Noise Characteristics of NACA0018 Airfoil," *Journal of Wind Engineering and Industrial Aerodynamics*, Vol. 95, No. 7, 2007, pp. 511–531. doi:10.1016/j.jweia.2006.11.002

[33] Corke, T. C., Post, M. L., and Orlov, D. M., "SDBD Plasma Enhanced Aerodynamics: Concepts, Optimization and Applications," *Progress in Aerospace Sciences*, Vol. 43, Nos. 7–8, 2007, pp. 193–217. doi:10.1016/j.paerosci.2007.06.001

[34] Opaits, D. F., Neretti, G., Likhanskii, A. V., Zaidi, S., Shneider, M. N., Miles, R. B., and Macheret, S. O., "Experimental Investigation of DBD Plasma Actuators Driven by Repetitive High Voltage Nanosecond Pulses with DC or Low-Frequency Sinusoidal Bias," AIAA Paper 2007-4532, 2007.

[35] Thomas, F. O., Corke, T. C., Iqbal, M., Kozlov, A., and Schatzman, D., "Optimization of Dielectric Barrier Discharge Plasma Actuators for Active Aerodynamic Flow Control," *AIAA Journal*, Vol. 47, No. 9, 2009, pp. 2169–2178. doi:10.2514/1.41588